Wu *et al. Earth, Planets and Space* (2016) 68:151
DOI 10.1186/s40623-016-0525-y

Earth, Planets and Space

FULL PAPER Open Access

The first super geomagnetic storm of solar cycle 24: "The St. Patrick's day event (17 March 2015)"

Chin-Chun Wu[1*], Kan Liou[2], Ronald P. Lepping[3], Lynn Hutting[1], Simon Plunkett[1], Russ A. Howard[1] and Dennis Socker[1]

Abstract

The first super geomagnetic storm (Dst < −200 nT) of solar cycle 24 occurred on "St. Patrick's day" (17 March 2015). Notably, it was a two-step storm. The source of the storm can be traced back to the solar event on 15 March 2015. At ~2:10 UT on that day, *SOHO/LASCO* C3 recorded a partial halo coronal mass ejection (CME), which was associated with a C9.1/1F flare (S22W25) and a series of type II/IV radio bursts. The initial propagation speed of this CME is estimated to be ~668 km/s. An interplanetary (IP) shock, likely driven by a magnetic cloud (MC), arrived at the *Wind* spacecraft at 03:59 UT on 17 March and caused a sudden storm commencement. The storm intensified during the Earth's crossing of the ICME/shock sheath and then recovered slightly after the interplanetary magnetic field (IMF) turned northward. The IMF started turning southward again due to a large MC field itself, which caused the second storm intensification, reaching a minimum value (Dst = −223 nT). It is found that the first step is caused by a southward IMF component in the sheath (between the upstream shock and the front of the MC), whereas the second step is associated with the passage of the MC. The CME that erupted on 15 March is the sole solar source of the MC. We also discuss the CME/storm event with detailed data from observations (*Wind* and *SOHO*) and our algorithm for predicting the intensity of a geomagnetic storm (Dst_{min}) from known IP parameter values. We found that choosing the correct Dst_{min} estimating formula for predicting the intensity of MC-associated geomagnetic storms is crucial for space weather predictions.

Keywords: Coronal mass ejection, Interplanetary shock, Super geomagnetic storm, Magnetic cloud

Introduction

Geomagnetic storms can be categorized, in terms of geomagnetic activity index (Dst), into three categories: (1) major (intense or great) storms, minimum Dst (Dst_{min}) of −100 nT or less; (2) moderate storms, Dst_{min} falls between −50 and −100 nT; and (3) weak storms, −30 nT < Dst_{min} < −50 nT (Gonzalez et al. 1994). Major geomagnetic storms that occurred in solar cycle 23 have been studied comprehensively (Zhang et al. 2007). It was found that ~85 % of major geomagnetic storms were associated with interplanetary (IP) coronal mass ejections (ICMEs) (Zhang et al. 2007), and the average storm intensity ($\langle Dst_{min} \rangle$) was typically larger for magnetic cloud (MC) events and smaller for non-cloud ICME or corotating fast flow events. The tendency is more pronounced for events associated with X class flares (e.g., Wu et al. 2013). The definition of a "super-storm" varies in the science community. For example, Astafyeva et al. (2014) used Dst_{min} < −250 nT as a super-storm but Lakhina and Tsurutani (2016) used Dst_{min} < −500 nT as a super-storm. Here we call a geomagnetic storm a super-storm when Dst_{min} drops below −200 nT.

Geomagnetic storms are major space weather events. A geomagnetic storm can affect space vehicle operation, interrupt radio communication, and disrupt power grids. During the last solar minimum, 2007–2009, the sunspot number (SSN) was extremely low and no major geomagnetic storm was recorded. The largest geomagnetic storms recorded in 2007, 2008, and 2009 were (Dst_{min}) −70, −72, −79 nT, respectively. The first geomagnetic

*Correspondence: chin-chun.wu@nrl.navy.mil
[1] Naval Research Laboratory, Washington, DC 20375, USA
Full list of author information is available at the end of the article

storm ($Dst_{min} < -73$ nT) associated with a coronal mass ejection (CME) and a driven shock in solar cycle 24 occurred on 6 April 2010, which was associated with a CME event on 3 April 2010 (e.g., Möstl et al. 2010; Liu et al. 2011; Wood et al. 2011).

The first major geomagnetic storm in solar cycle 24 occurred during 05–06 August 2011 ($Dst_{min} = -107$ nT), and the second and third major geomagnetic storms occurred during 26–27 September 2011 [$Dst_{min} = -101$ nT (e.g., Wu et al. 2016a)] and 24–25 October 2011 ($Dst_{min} = -132$ nT), respectively (e.g., Wood et al. 2016). There were five major geomagnetic storms recorded in 2012 alone, but only two major geomagnetic storms were recorded in 2013: one ($Dst_{min} = -132$ nT) on 17 March 2013 (Wu et al. 2016b) and the other one on 1 June ($Dst_{min} = -119$ nT). In the early phase of solar cycle 24, the most intense storm occurred during 07–08 March 2012. This storm's Dst_{min} reached −143 nT. The first super geomagnetic storm of solar cycle 24 did not occur until the declining phase on 17 March 2015 (e.g., Gopalswamy et al. 2015; Kamide and Kusano 2015; Kataoka et al. 2015; Liu et al. 2015; Ramsingh et al. 2015).

It is well known that the southward component of the interplanetary magnetic field (IMF) plays a major role in the generation of geomagnetic storms (e.g., Tsurutani et al. 1988; Tsurutani 1997). A large southward IMF can be associated with different kinds of solar wind structures: (1) an interplanetary (IP) shock wave (sheath) (e.g., Tsurutani et al. 1988; Kamide et al. 1998; Wu and Lepping 2008, 2016), (2) a magnetic cloud (MC) (e.g., Wu and Lepping 2002a, b) or an IP coronal mass ejection (ICME) (e.g., Richardson and Cane 2011; Wu and Lepping 2011), (3) a heliospheric current sheet sector boundary crossing (e.g., McAllister and Crooker 1997), or (4) a combination of these interplanetary structures (e.g., Tsurutani and Gonalez 1997; Echer and Gonzalez 2004). Among these, MCs are the most geoeffective because they generally contain a large, long-lasting southward IMF (e.g., Wu and Lepping 2008, 2016). About 90 % of MC events are associated with geomagnetic storms. A MC event includes the MC itself, usually an upstream shock wave with a sheath (region between the shock and the MC) (e.g., Wu and Lepping 2002a, 2011; Wu et al. 2015). Most solar cycle 23 major storms (88 of them) are associated with an ICME or an MC (Zhang et al. 2007; Wu et al. 2013).

A geomagnetic storm can be induced by (1) the MC sheath, (2) the leading (i.e., front part) region of a MC, (3) the trailing part of an MC, and (4) both sheath and MC regions (e.g., Wu and Lepping 2002a). It is found that the minimum value of the z component of the IMF ($B_{z_{min}}$) within a MC is well correlated with the intensity of a geomagnetic storm (Dst_{min}) (e.g., Wu and Lepping 2002a, 2002b, 2015, 2016); we consider the z_{GSE}-component. Therefore, measurements of $B_{z_{min}}$ in the solar wind can be used to predict Dst_{min} (e.g., Wu and Lepping 2016).

The St. Patrick's Day geomagnetic storm was associated with a CME event that occurred on 15 March 2015. At ~2:10 UT on that day, *SOHO/LASCO* C3 recorded a partial halo CME, which was associated with a C9.1/1F flare (S22W25) and a series of type II/IV radio bursts. Notably, this event was a two-step storm. It serves as a good candidate to evaluate the effectiveness of our Dst estimation formulae (Wu and Lepping 2016). Data analysis is presented in "Observations". Discussion and Conclusion are presented in "Discussion" and "Conclusion" section.

Observations

Propagation of CMEs near the Sun

Figure 1 shows a sequence of white-light coronal images recorded by SOHO/LASCO C2 during 00:00–03:12 UT on 15 March 2015. C2 recorded a CME (named CME15, hereafter) that erupted from the southwest at 01:48 UT (Fig. 1b) and appeared as a partial halo CME during 02:12–03:12 UT (Fig. 1d–h) in the field of view (FOV) of C2. CME15 was associated with a C9.1/1F flare (S22W25) and a series of type II/IV radio bursts. The initial propagation speed of CME15 was ~606 km/s (see Fig. 2). SOHO/LASCO C3 recorded the CME15 at 02:18 UT (Fig. 3a) in the FOV. Figure 3a–c shows the evolution of CME15 during 02:18 UT–06:06 UT on 15 March 2015. The average speed of CME15 in the C3 FOV was 668 km/s.

In situ observation at L1

Figure 4 shows the in-situ solar wind plasma, magnetic field (measured by the *Wind* spacecraft), and the Dst index during 16–18 March 2015. The *Wind* spacecraft recorded an interplanetary (IP) shock (we will refer to this shock as Shock17, marked by a solid vertical line in Fig. 4) at 03:57 UT on 17 March 2015, and a flux-rope candidate a few hours after the crossing of Shock17. Using a MC-fitting model (Lepping et al. 1990), Table 1 lists the best-fit results for the MC (we will refer to this MC as MC17). Figure 5a, b shows MC17's magnetic field structure in cloud coordinates and GSE coordinates, respectively. The solid-black curves are the MC-fitting results. MC17 started at 10:36 UT (marked by a vertical dashed line with a sharp change in B_y and ϕ_B) and ended at 23:36 UT (marked by a vertical solid line where there is a sharp drop in $|B|$) on 17 March. The boundaries of a MC are usually indicated by sharp changes in field angle (θ_B or ϕ_B) or in field magnitude, $|B|$. The duration (Δt_{MC}) of MC17 is 13.00 h, which is ~30 % smaller than an average MC at 1 AU, $\Delta t_{MC} = 18.82$ h, (e.g., Lepping et al. 2015; Wu and Lepping 2015). The duration of the sheath is about 7 h. The MC17 fitting results are showed

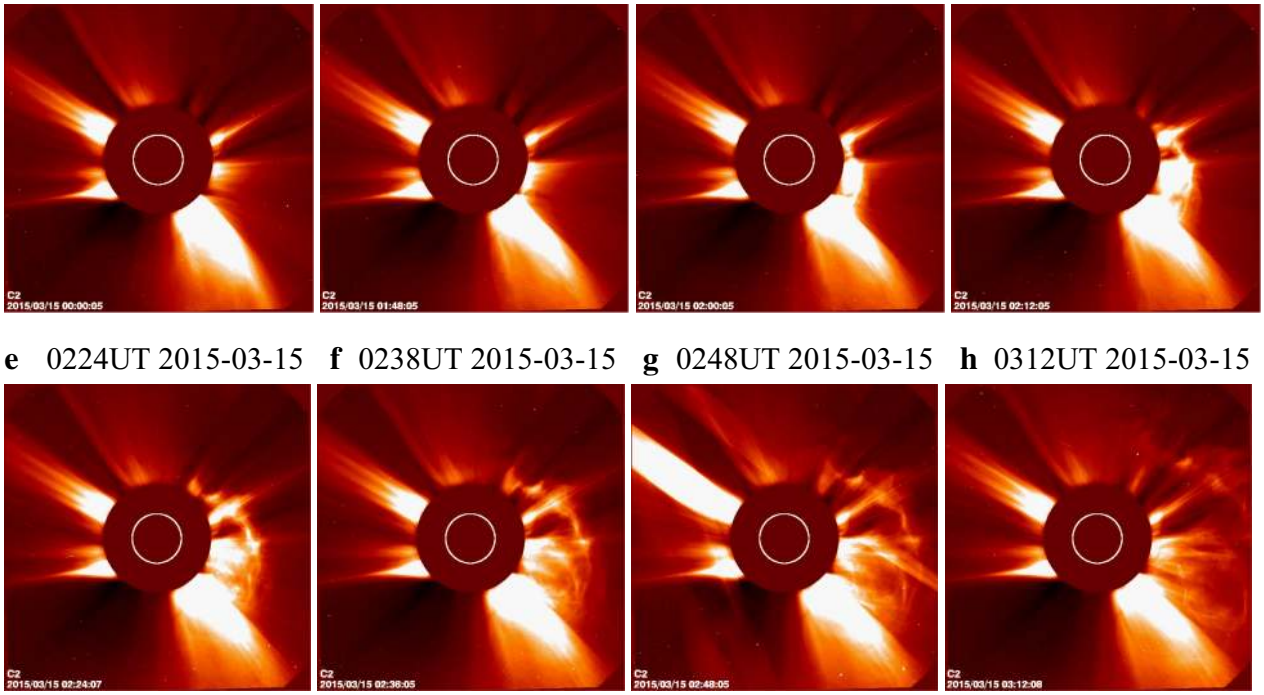

Fig. 1 Coronal images recorded by SOHO/LASCO C2 during 00:00–03:12 UT (**a**–**h**) on 15 March 2015. At 0148 UT (**b**) C2 recorded a CME that erupted from the southwest

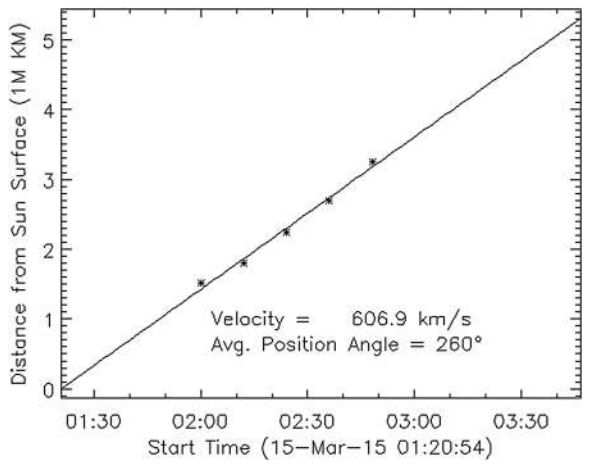

Fig. 2 Propagation speed of the CME on 15 March 2015: The average speed at the middle (*center*) of the CME is ~606 km/s

in both Fig. 5 and Table 1. As we see, especially in cloud (CL) coordinates, the directional part of the fit is between fair and good, but the B-magnitude part of the fit is poor: There is a double peak in the observation but not in the model. The model-field center of the MC17 was in the actual center (see bottom panel of Fig. 5a for the profile of ϕ_B), and θ_B is almost flat (second panel from bottom) as required in cloud coordinates. However, according to the definition of MC quality (Q_o) (Lepping et al. 2006), we classify MC17 as a quality 3 MC, because the MC's magnetic field noise level, χ_R (Lepping et al. 2003), was high ($\chi_R = 0.244$). If a MC's χ_R is greater than 0.215, the quality of that MC will be 3.

The arrival of Shock17 at the Earth produced a sudden storm commencement (SSC) at 04:45 UT. The value of Dst started decreasing right after the IMF turned southward. The storm intensified (Dst dropped to −80 nT at ~10:00 UT) during the passage of the sheath (a region between the IP shock and the driver of the IP shock). Later, the storm recovered slightly (i.e., Dst dropped to ~ −50 nT), shortly after the IMF turned northward. A few hours later, the IMF turned southward again due to the strongly negative B_z in the magnetic cloud (MC) and caused the second storm intensification, reaching Dst = −223 nT on March 17. We conclude that the St. Patrick's day event (March 17) is a two-step storm. The first step was associated with a southward IMF embedded in the sheath region, whereas the second step was associated with a southward MC field.

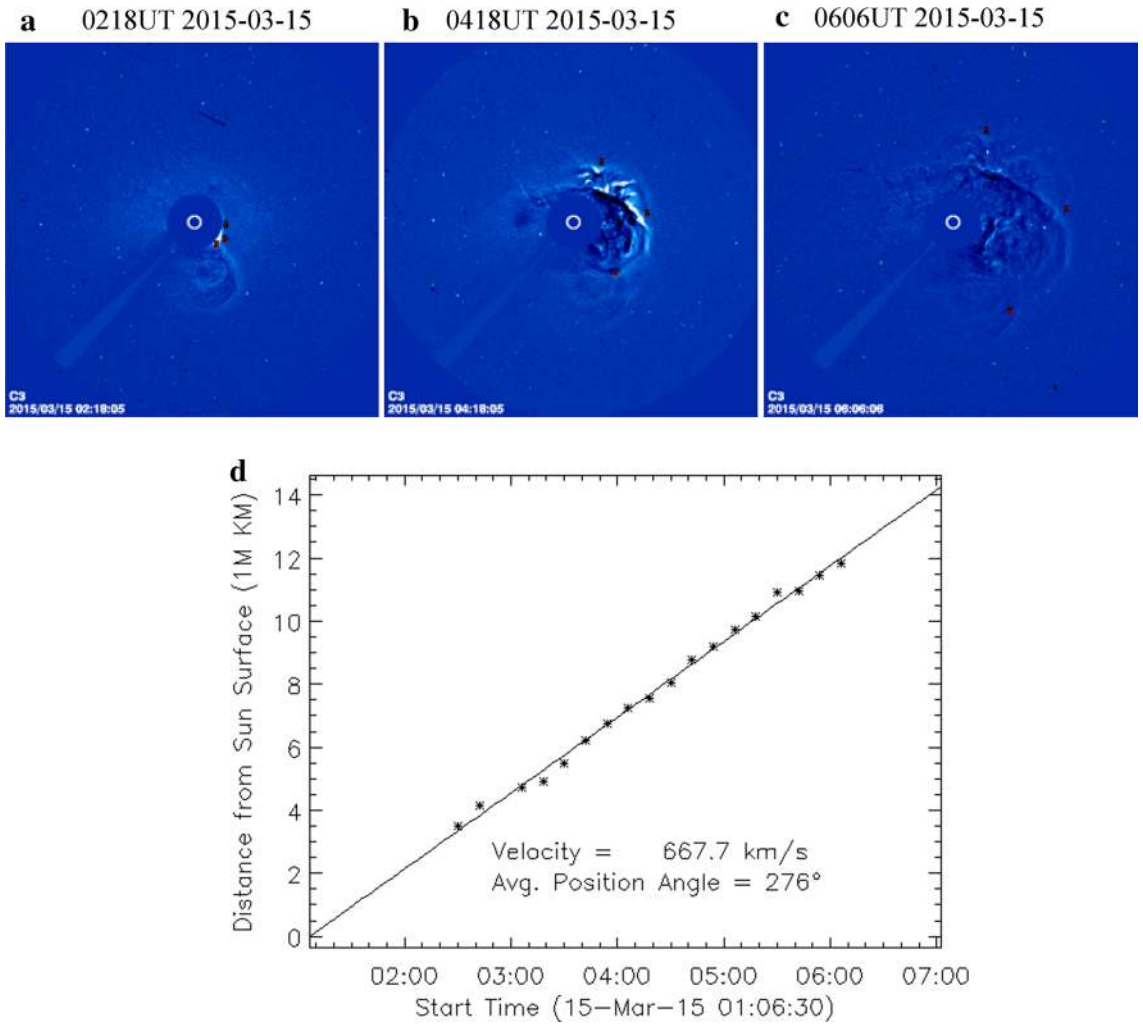

Fig. 3 **a**–**c** CME images recorded by SOHO/LASCO C3 during 02:18–06:06 UT on 15 March 2015. **d** Propagating speed of the CME in the field of view (FOV) of C3 is ~668 km/s

Propagation/evolution of the CME and its driven shock

The estimated speed of the CME varies, ranging from ~606 km/s in the C2 FOV (2.5–6.0 Solar radii, Rs), ~668 km/s in the C3 FOV (3.7–32 Rs), to ~706 km/s between 18.82 and 211 Rs ($V_{18.82-211Rs}$ = 706 km/s, at 06:06 UT on March 15, CME15's leading edge was at 18.82 Rs, see Fig. 3d). Note that the CME propagation speed measured by C2 or C3 was the projected speed on the plane of the sky. Although the projected speed has been corrected for the CME propagation direction, errors may still exist and contribute to the uncertainties in the arrival time predictions. Table 2 lists information about the location and the propagation speed of the CME and its driven shock. Note that the distances measured by C2 and C3 are those *above* the solar surface. These observations suggest that the propagating speed of the CME was similar in the both regions of 18.8–211 Rs and 6.95–18.8 Rs.

The estimated propagation speed of Shock17 and the ICME17 was 797 and 702 km/s in the area of 6.95–211 Rs, respectively. The in situ solar wind speed was ~400 and 500 km/s upstream and downstream of the IP shock, respectively. The speed in the sheath was between 500 and 600 km/s, and the average speed of the plasma over the entire MC was 550 km/s.

The estimated ICME propagation time to the Earth, based on C3 measurements, was ~58.96 h, i.e., "$204.05 \times 6.95 \times 10^5/(668 \times 3600) = 58.96$ h." This means that the ICME would arrive at the Earth at ~15:09 UT on 17 March 2015. The *Wind* measurements indicate that it took slightly less time (56.13 h) for the CME to propagate from Sun to 1 AU. The error on the propagation time

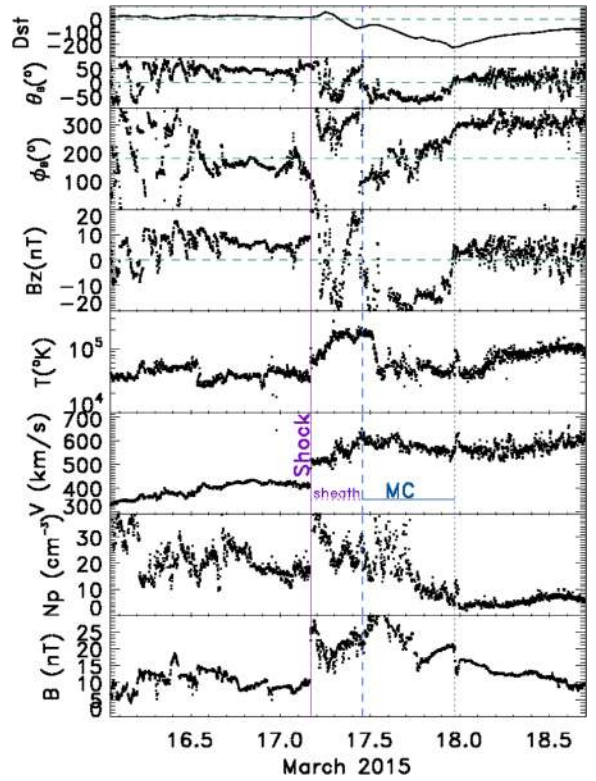

Fig. 4 Geomagnetic activity index (Dst: *top panel*) and *Wind* observed in situ solar wind parameters (*second–eighth panels*) during 16–18 March 2015. From *top* to *bottom* Dst, latitude (θ_B), and longitude (ϕ_B) of the magnetic field in GSE coordinates. B_z of the field in GSE, proton temperature (*T*), bulk speed (*V*), number density (*Np*), and magnetic field magnitude (*B*). The *blue horizontal line* in the third panel from the *bottom* represents the scheme's identification of the extent of this MC candidate (Lepping et al. 1990). The *purple-solid line* and *blue-dashed vertical lines* represent the IP shock and the front boundary of the MC, respectively

Table 1 MC fit-parameters for the MC of 17 March 2015 (starting day)

Starting time = 10:38 UT	CA (%) = −3 %
$\Delta T = 13.0$ h	$\Delta t = 15$ min
$V_{MC} = 550$ km/s	$\beta_{CA} = 116°$
$2R_o = 0.166$ AU	Check = −6.4 %
$B_o = 25.65$ nT	$\Phi_o = 5.4 \times 10^{20}$ Mx
$H = +1$ right-handed	$J_o = 4.0$ μA km^{-2}
$\theta_A = -63°$ and $\phi_A = 162°$ (GSE coordinates)	$I_T = 8.3 \times 10^8$ A
$\chi_R = 0.244$	$N = 54$
Asf (%) = 9.7 %	$Q_o = 3$

ΔT, duration of the MC encounter (i.e., ΔT = end time – start time of MC passage); V_{MC}, average solar wind speed (in km s^{-1}) within the MC; $2R_o$, estimated diameter (in AU), where R_O is the model-estimated radius; B_O, estimated axial magnetic field magnitude (in nT); *H*, Handedness (+1 for right-handed or −1 for left-handed); ϕ_A, θ_A, longitude and latitude, respectively, of the MC axis (GSE coordinates); t_o, estimated center time of the MC; χ_R, square root of the reduced Chi-squared of the MC fit; asf(%), asymmetry factor (in %), which depends on t_o and ΔT; CA (%), estimated relative closest approach distance, i.e., y_o/R_o (in %) where y_o is closest approach; Φ_o, estimated axial magnetic flux (in 10^{20} Mx); J_O, estimated total axial current density (in μA km^{-2}); Δt, length of the averages used in the analysis; these are usually 15, 30 min, or 1 h; β_{CA}, cone angle, the angle between the MC axis and the *X*-axis (in GSE coordinates); "Check," a check of the estimated radius by using duration, speed, CA, cone angle, and R_o; I_T, estimated total axial current (in 10^8 A); *N*, number of points used in the MC-fitting interval; Q_o, estimated quality of the model fitting (where $Q_o = 1$, 2, or 3, for excellent, good, or poor, respectively)

is ~5 % if 668 km/s was used as an estimate of the CME speed, i.e., "(58.96–56.13)/56.13 ≡ 5 %." Therefore, the March 15 CME was clearly responsible for the generation of the Shock17 and the St. Patrick's Day storm. In addition, the CME speed measured by C3 is good to use for estimating the ICME's arrival time at the Earth. The speed of the CME that occurs near the Sun is usually inferred to be faster than it is in interplanetary space.

Discussion

One may argue about the importance of the prediction of the SAT (shock arrival time at the Earth) because interplanetary shocks do not cause geomagnetic storms directly. However, structures behind shocks, in the sheath, do cause geomagnetic storms frequently. For example, the shocks' drivers, MCs, are one of the most geo-effective IP structures (e.g., Wu and Lepping 2016 and references therein). Using statistical studies of *Wind* data (1995–2012), Wu and Lepping (2016) found: (1) the average intensity of geomagnetic storms ($\langle Dst_{min} \rangle$) associated with IP shocks, MCs, and magnetic cloud like structures (MCLs) are −78, −70, and −35 nT, respectively; (2) the $\langle Dst_{min} \rangle$ for MC_{shock} (MCs with upstream shock waves) and $MC_{no\text{-}shock}$ (MC without upstream shock wave) events are −102 and −31 nT, respectively; and (3) the average duration of the sheath (the area between an IP shock and the front boundary of MC) is about 12 h long.

Interplanetary shock/CME arrival time at the Earth

The propagation speeds of CME15 were 606 (V_{C2}) and 668 (V_{C3}) km/s in the FOV of LASCO/C2 and C3 (see Table 2). The estimated shock (or CME) arrival times (SAT) at the Earth were 65.89 h for V_{C2} and 58.96 h for V_{C3}. It took about 49.45 and 56.13 h for Shock17 and ICME17 to arrive at the Earth, if V_{C3} is used. But SAT was 65.89 h if V_{C2} is used. Δt_{ERR} were 16, 5 % for $SAT_{Shock17}$ and SAT_{MC17}, if V_{C3} is used. Δt_{ERR} were 30, 15 % for $SAT_{Shock17}$ and SAT_{MC17}, if V_{C2} is used. Therefore, the measurement of V_{C2} (or V_{C3}) is very important for space weather. The speed of V_{C2} (or V_{C3}) represented the speed of the "driver" of the shock, not the speed of the "shock." The results of this study suggested that "using the right CME propagation speed is essential for space weather prediction."

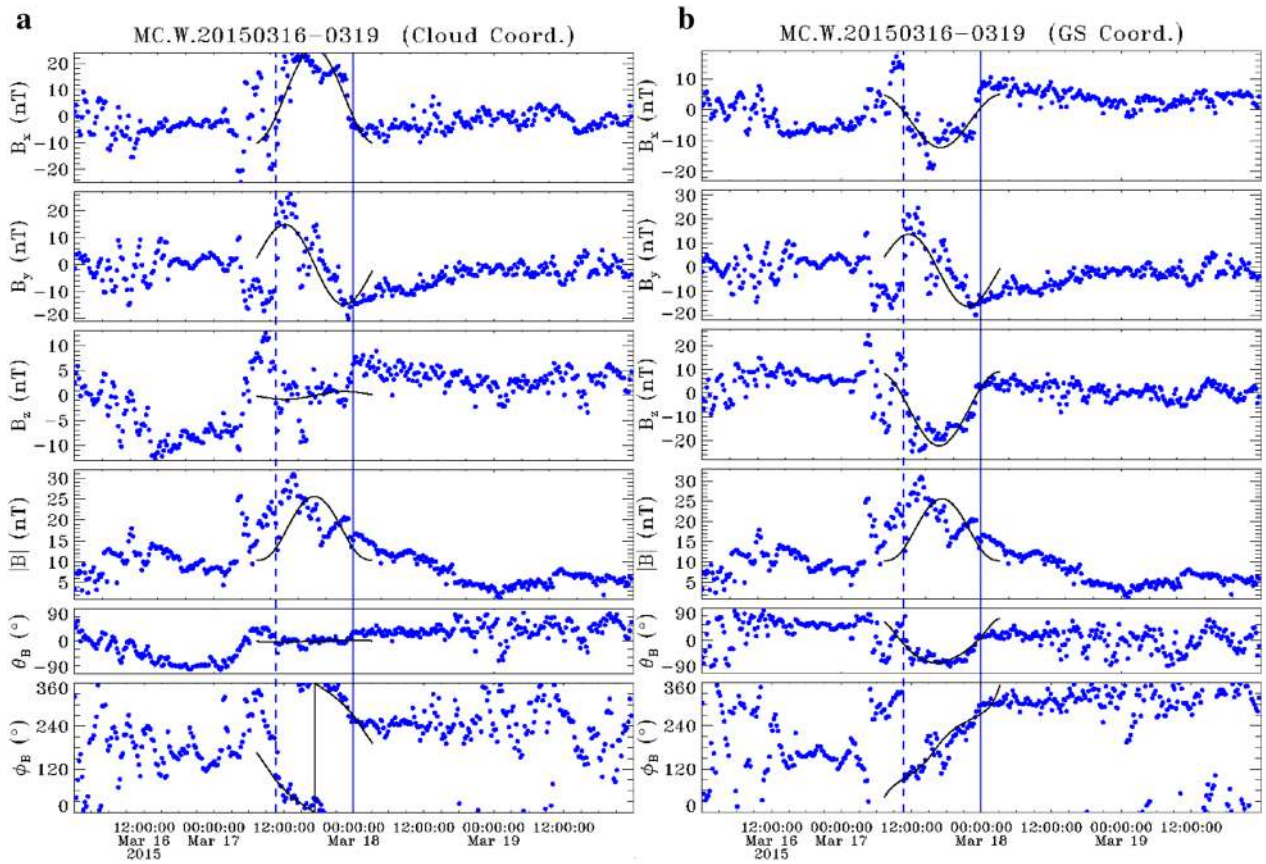

Fig. 5 MC of 17 March 2015. This is a good-quality ($Q_o = 1$) example of the use of the Lepping et al. (1990) MC-fitting model where the points are the observed magnetic field data (in 15 min average form), and the *solid-black curves* are the result of the model. **a** The *left six panels* are given in the cloud coordinates (CL) in terms of magnetic field in *x*-, *y*-, *z*-components (B_x, B_y, B_z), field intensity ($|B|$), latitude (θ_B), and longitude (ϕ_B), and **b** the *right six panels*, for the same physical quantities, are in geocentric-solar-ecliptic (GSE) as designated. The *dashed vertical line* is the estimated MC start-time (see Table 2), and the *solid vertical line* is the estimated end time

One can use the V_{CME} (e.g., V_{C2} or V_{C3}) value to estimate the arrival time of the driver's front boundary first. Then use the duration of sheath (~12 h) to estimate the SAT if there is an IP shock in front of the driver.

Is the intensity of a geomagnetic storm predictable?

The prediction of geomagnetic storm intensity is one of the most important goals in space weather. A severe geomagnetic storm can affect the operation of a space vehicle, interrupt telecommunication around the world, and/or damage power grids on the ground. For example, power plants in Canada were damaged by a storm that occurred in March 1989.

The minimum *Bz* ($B_{z_{min}}$) was −23 nT (in GSE coord.) while the Wind spacecraft passed through MC17. $B_{z_{min}}$ occurred in the front portion of the MC17. The average solar wind speed ($\langle V \rangle$) was ~500 km/s in the sheath and ~600 km/s inside the MC17. Many empirical formulae for estimating Dst_{min} are available (e.g., Wu and Lepping 2005, 2015, 2016; Gopalswamy et al. 2015). Tables 3 and 4 list formulae for the estimation of Dst that were derived from extensive *Wind* MC data sets [Dst_{min} formulae were obtained from Tables 6, 7, and 8 of Wu and Lepping (2016)]. The estimated Dst_{min} from these formulae were in a range between −129 and −240 nT for the St. Patrick's Day Storm, with errors $|(Dst_{obs}-Dst_{pred.})/Dst_{obs.}|$ in a range of 3–50 %.

Without considering solar wind velocity, the best prediction of Dst_{min} was −179.7 nT (error = 21.2 %) by using a Dst formula derived from 83 MCs that occurred during 1995–2003 (g in Table 3). Using a speed dependent Dst_{min} formula, the predicted Dst_{min} was in a range of −121 to −240 nT, and the errors were in a range between 2.9 and 49.6 % (Table 4). The best three predictions are −218.2, −221.4, and −239.9 nT (errors are 4.3, 2.9, and 5.2 %) by using Table 4's Dst formulae (3), (4), and (9), respectively. "Best prediction" means that the predicted Dst_{min} has the smallest error. It has been shown that

Table 2 Related information for the CME15, Shock and ICME17 during 15–17 March 2015

	Start time[a] UT (Mar. 15)	r[b] Rs	Ending time[c] UT (Mar. 17)	Δr[d] Rs	Δt[e] (h)	$V_{shock/CME}$[f] (km/s)	V'[g] (km/s)	Δt_{pred}[h] (h)	Δt_{ERR}[i] (h) (%)
$Shock_{C3}$	2:30	6.95–18.82	03:57	204.05	49.45	796.6	668	58.97	16
$ICME_{C3}$	2:30	6.95–18.82	10:38	204.05	56.13[j]	701.8	*668*	*58.96*[k]	*5*[l]
$Shock_{C2}$	2:00	4.15–6.61	03:57	206.85	49.95	799.5	606	65.00	30
$ICME_{C2}$	2:00	4.15–6.61	10:38	206.85	56.63	705.0	606	65.00	15

[a] CME/shock was observed by SOHO/LASCO

[b] Location of leading edge of CME measured by C3 or C2 (units in Rs)

[c] Starting point at 1 AU (*Wind*)

[d] Distance between the initial point observed by C3 and *Wind* (units in Rs), and 1 Rs $= 6.95 \times 10^5$ km

[e] Δt: traveling time of shock/CME between 6.95 Rs and 1 AU (units in hours), and 1 AU equals to 215 Rs

[f] $V_{shock/CME} = \Delta r/\Delta t$ (units in km/s)

[g] V': $V_{CME/shock}$ measured near the Sun between 6.95 and 18.82 Rs (units in km/s)

[h] $\Delta t_{prediction}$: predicted traveling time for shock/CME propagating from 6.95 Rs to Wind (units in hours)

[i] Δt_{ERR}: error on the $\Delta t_{pred} = (\Delta t_{pred} - \Delta t)/\Delta t \times 100$ (%)

[j] Traveling time of ICME17 from 6.95 Rs to *Wind* spacecraft, ICME was seen by C3 at 2:30 UT on 15 March and recorded by Wind at 10:38 UT on 17 March [$\Delta t = 2 \times 24 + (10–2) + (38–30)/60 = 56.13$ h]. Wind orbited at 258.7 R_E (GSE). Earth was at 213.938 Rs. Wind was at ~211 Rs (GSE). Therefore $V_{CME} = \Delta r/\Delta t = (204.05$ Rs/56.13 h) $= 701.8$ km/s

[k] $204.05 \times 6.95 \times 10^5/(668 \times 3600) = 58.96$ h

[l] $(58.96-56.13)/56.13 \equiv 5$ %

Table 3 Estimated Dst_{min} based on formulae obtained from Wu and Lepping (2016) for a MC event that occurred on 17 March 2015

	Event	Dst_{min} formula[a]	*Pred.* Dst_{min}[b]	Source of $B_{z_{min}}$[c]	Errors (%)
(a)	168 MCs	$Dst_{min} = -3.30 + 6.82 \times B_{z_{min}}$	*−160.2*	*MC*	*29.8*
(b)	168 MCs	$Dst_{min} = 8.04 + 6.34 \times B_{z_{min}}$	−137.8	Sheath or MC	39.6
(c)	*94 MC_{SHOCK}*	$Dst_{min} = -22.89 + 6.12 \times B_{z_{min}}$	*−163.7*	*MC*	28.2
(d)	94 MC_{SHOCK}	$Dst_{min} = 11.01 + 6.47 \times B_{z_{min}}$	−137.8	Sheath or MC	39.6
(e)	94 MC_{SHOCK}	$Dst_{min} = -21.18 + 5.26 \times B_{z_{min}}$	−142.2	Sheath	37.6
(f)	74 $MC_{NOSHOCK}$	$Dst_{min} = 4.18 + 5.83 \times B_{z_{min}}$	−129.9	MC	43.0
(g)	83 $MC_{1995–2003}$	$Dst_{min} = 0.83 + 7.85 \times B_{z_{min}}$	−179.7	MC	*21.2*

[a] Linear-fitted function for Dst_{min} obtained from Wu and Lepping (2016)

[b] Predicted Dst_{min} by using Dst_{min} formula listed in the left

[c] $B_{z_{min}} = -23$ nT within the MC event recorded from wind spacecraft

Italics: the "best prediction" (with the lowest error) for Dst_{min}

Dst_{min} versus $B_{z_{min}}$ has a higher correlation for the MCs associated with higher solar wind speed than those with lower speed (e.g., Wu and Lepping 2002b, 2016). Using the empirical relationship ($Dst = -0.017\ VBz + 16$ nT), Gopalswamy et al. (2015) estimated $Dst_{min} = -239$ nT by using in $V = 600$ km/s, and $B_z = -25$ nT for this event. The estimated Dst_{min} was close to the observation. Solar wind speed is an important parameter for estimating geomagnetic storm intensity, as is well known.

How many MCs were associated with the super-storm of 17 March 2015?

We only identified MC17 as the driver for the IP Shock17 of 17 March 2015. The MC17 was identified in two procedures: (1) We first applied the automatic MC auto-identification (MCI) model (Lepping et al. 2005) to find the MC candidate, and then (2) we used a MC-fitting (MCF) model (Lepping et al. 1990) to determine the MC parameters. Figure 6 shows the time profile of the

Table 4 Estimated Dst_{min} based on formulae obtained from Wu and Lepping (2016) with $B_{z\,min} = -23$ nT

Range of MC's averaged speed[a]	Estimating Dst formula using $B_{z\,min}$ in MC[b]	Pred. Dst^{c}_{min}	Error (%)[d]	Estimating Dst formula using $B_{z\,min}$ in MC or sheath[b]	Pred. Dst^{c}_{min}	Error (%)[d]
1. $V < 400$[a]	$Dst_{min} = 12.12 + 6.55B_{z\,min}$	−138.5	39.3	11. $Dst_{min} = 14.19 + 6.52B_{z\,min}$	−135.8	40.4
2. $400 < V < 500$	$Dst_{min} = -21.08 + 4.82B_{z\,min}$	−131.9	42.1	12. $Dst_{min} = -16.14 + 4.50B_{z\,min}$	−119.6	47.5
3. $500 < V < 600$	*$Dst_{min} = -9.31 + 9.08B_{z\,min}$*	*−218.2*[e]	*4.3*	13. $Dst_{min} = 28.94 + 8.23B_{z\,min}$	*−160.4*	*29.6*
4. $600 < V < 750$	*$Dst_{min} = -70.76 + 6.55B_{z\,min}$*	*−221.4*	*2.9*	14. $Dst_{min} = 36.18 + 8.65B_{z\,min}$	−162.8	28.6
5. $V > 750$	$Dst_{min} = -147.07 + 2.84B_{z\,min}$	−212.4	6.8	15. $Dst_{min} = -32.14 + 4.54B_{z\,min}$	−136.6	40.1
94 MC_{shock}						
6. $V < 400$	$Dst_{min} = 12.28 + 6.82B_{z\,min}$	−144.5	36.6	16. $Dst_{min} = -10.83 + 5.42B_{z\,min}$	−114.8	49.6
7. $400 < V < 500$	$Dst_{min} = -43.37 + 3.37B_{z\,min}$	−120.9	47.0	17. $Dst_{min} = -36.69 + 3.21B_{z\,min}$	−111.7	51.0
8. $500 < V < 600$	$Dst_{min} = -54.55 + 4.72B_{z\,min}$	−163.1	28.5	18. $Dst_{min} = -13.01 + 5.14B_{z\,min}$	−132.8	41.8
9. $600 < V < 750$	$Dst_{min} = -66.72 + 7.53B_{z\,min}$	−239.9	*5.2*	19. $Dst_{min} = 75.96 + 10.43B_{z\,min}$	−191.2	16.1
10. $750 < V$	$Dst_{min} = -147.07 + 2.84B_{z\,min}$	−212.4	6.8	20. $Dst_{min} = -32.14 + 4.54B_{z\,min}$	−141.9	37.9

[a] Range of averaged speed inside of the MC

[b] Linear-fitted function for Dst_{min} obtained from Wu and Lepping (2016)

[c] Predicted Dst_{min} by using Dst_{min} formula listed in the left

[d] Error = $|(Dst_{obs} - Dst_{pred.})/Dst_{obs.}|$

[e] $Dst_{prediction} = -218.2$ nT ($B_{z\,min} = -23$ nT) using Dst_{min} formula 3) for $500 < V < 600$ km/s

Italics: the "best prediction" (with the lowest error) for Dst_{min}

interplanetary magnetic field, solar wind plasma, Dst index, and some derived parameters during 17–18 March 2015. The MCI model identified a MC candidate, which is marked by a horizontal black bar, and the MCF model was able to identify a MC (MC17), which is bounded between two vertical red lines, as shown in Fig. 6d. The rear boundary of the MC17, as determined visually, is consistent with that determined by the MCI model, but the MC17 front boundary, as determined visually, is about 4 h ahead of that determined by the MCI model. The shock driven by the MC17 (Shock17) is marked by a vertical line in Fig. 6.

Wind recorded ~24 h of low plasma beta (β) solar wind material between ~12:00 UT on March 17 and ~12:00 UT on March 18. The low β region was separated by a magnetic hole, which occurred at the end of 17 March (indicated by dotted and dashed lines). Behind the MC17's rear boundary, there was a ~12-h low β interval (marked in orange color and "ICME ?" in Fig. 6b). Using the MCF model, we are not able to obtain a good fit for this region because the magnetic field did not vary much in direction (i.e., θ_B or ϕ_B did not change much) inside this region (see Fig. 6e, f). Besides the absence of significant field rotation in that region, B_z was almost zero in that period. Therefore, we concluded that the superstorm on 17 March 2015 was caused by the southward field in both the sheath and the MC17.

The results of this study are consistent with the recent work by Kataoka et al. (2015), but are different from the results concluded by Gopalswamy et al. (2015), or Liu et al. (2015). The MC interval identified by Gopalswamy et al. (2015) is almost double the interval of MC17. Liu et al. found that there were two ICMEs associated with the storm of 17 March by using the best Grad–Shafranov-fit model, and both ICMEs were flux-ropes (FRs) [see Fig. 2 of Liu et al. (2015)].

Liu et al. asserted that an IMCE (ICME1) occurred with an ending point about several hours ahead of MC17 and a second ICME (ICME2) started right after the end of ICME1. In addition, a magnetic hole was found in the middle of ICME2 about 4 h behind the front boundary of ICME2. Often, a magnetic hole marks the boundary of a MC. The MCF model used in this study is not expected to be able to not find a good fit since there is a magnetic hole inside the fitting region. Liu et al. used a different ICME fitting model to fit their ICME2 and chose a different period for their study (Liu et al. 2015). Our MC's boundaries do not agree with their ICMEs' boundary selections. Based on the discussion above, we concluded that there was only one MC and one MC's driven shock associated with the superstorm on 17 March 2015.

Many MC or flux-rope fitting models are available in the science community (e.g., Hua and Sonnerup 1999; Marubashi and Cho 2015; Möstl et al. 2009; Lepping et al. 1990; Wang et al. 2015). It would be useful to know whether and/or how they perform differently. However, this is beyond the scope of this study.

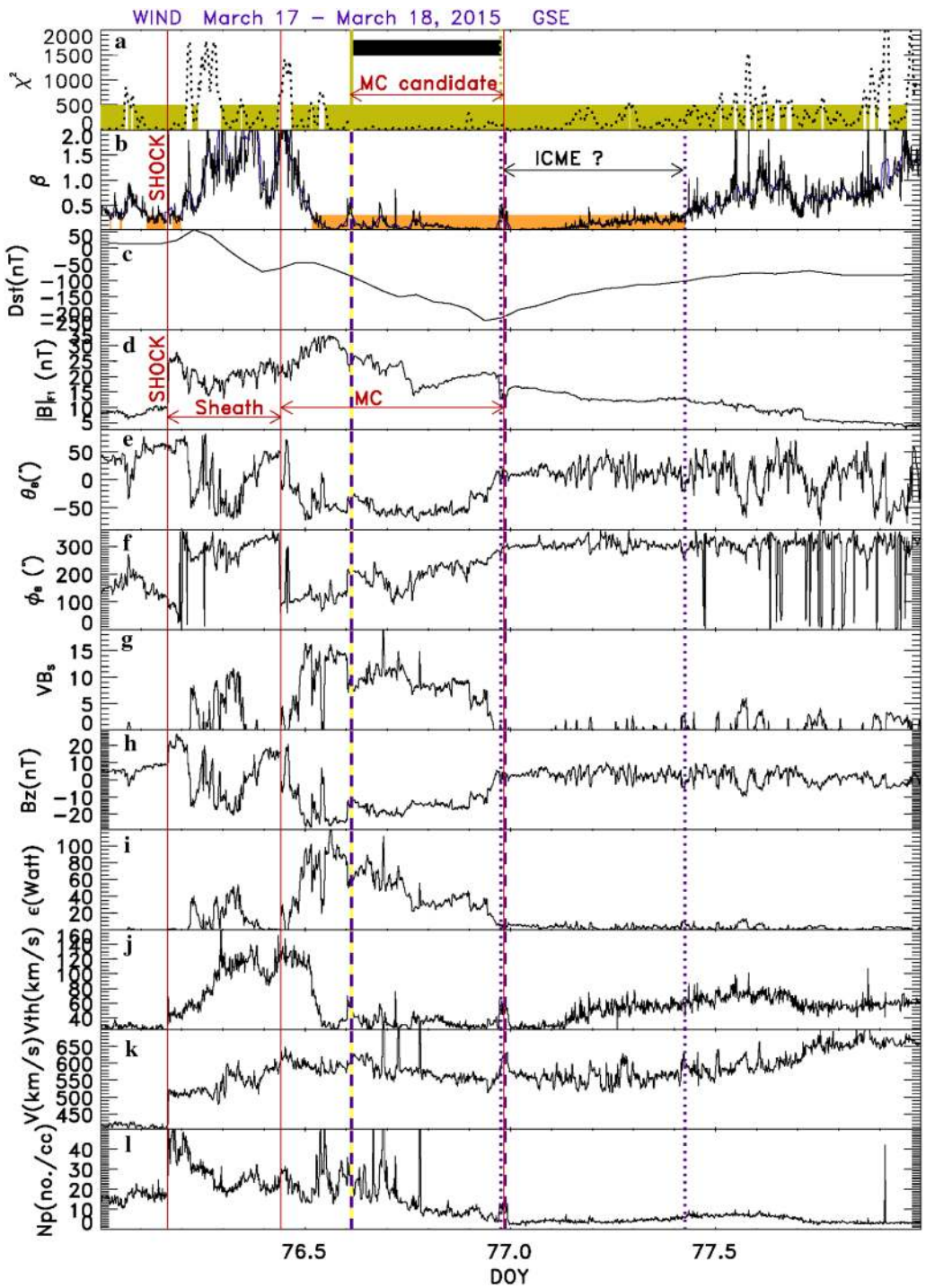

Fig. 6 Profile of magnetic field and plasma parameters for S-N MC of 17 March 2015, in terms of (from *top* to *bottom*, **a**–**l**): χ^2 of a quadratic fit to latitude of the filed (θ_B), running average of proton plasma beta (β), Dst index, magnetic field in terms of magnitude, latitude (θ_B) and longitude (ϕ_B) in GSE cords., induced electric field (VBs), B_z of the field in GSE, $\boldsymbol{\varepsilon}$ (see, Akasofu 1981), proton plasma thermal speed (V_{Th}), bulk speed (V), and number density (N_{p}). One MC candidate was marked on (*a*). In (*d*), an IP shock was indicated by a *vertical red-solid line*; sheath was bounded between the *two red-vertical-solid lines*; MC was marked in (*d*). In (*a*), $\chi^2 < 500$ was marked in *yellow*

Solar source of the super-storm on 17 March 2015

The solar source of the super-storm of 17 March 2015 is a hot topic for some science communities [e.g., the International Study of Earth-affecting Solar Transients (ISEST) for Variability of the Sun and Its Terrestrial Impact (VarSITI)]. In order to answer the question, earlier CME images were checked and a slow CME was identified on 14 March 2015 (We will refer this CME as CME14). CME14 was first seen at 17:43 UT by SOHO/LASCO C3. Figure 7 shows a sequence of CME images recorded by SOHO/LASCO C3 between 17:42 UT on 14 March and 09:06 on 15 March 2015. The "+" and "*" symbols indicate the leading edge of CME14 and CME15 (this CME erupted on 15 March 2015), respectively. The speed of CME14 was very slow (~240 km/s, see Fig. 8). Figure 7e shows that CME15 was recorded by C3 on the right (or west), and CME14 was at the bottom (or south). The leading edge of CME15 passed the leading edge of CME 14 (see Fig. 7g–j) after 06:30 UT on 15 March.

Previous studies suggested that the storm on 17 March 2015 may be caused by the interaction between two successive CMEs plus the compression by a high-speed stream from behind (e.g., Liu et al. 2015). Our interpretation of the coronagraph images is different

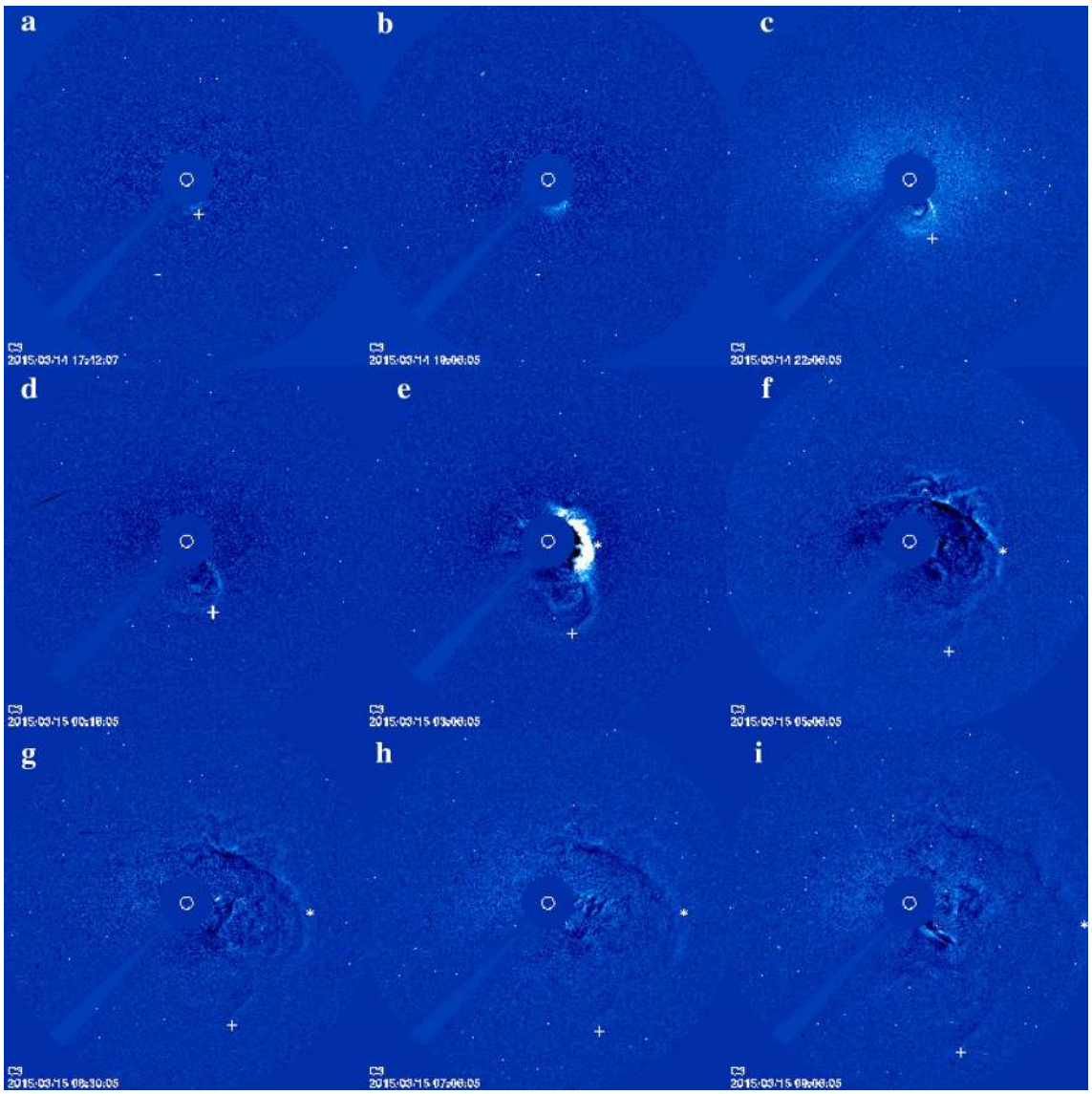

Fig. 7 CME images recorded by SOHO/LASCO C3 during 17:42 UT on 14 March and 09:06 on 15 March 2015. "+" and "*Asterisk*" indicate the leading edge of CME14, and CME15, respectively

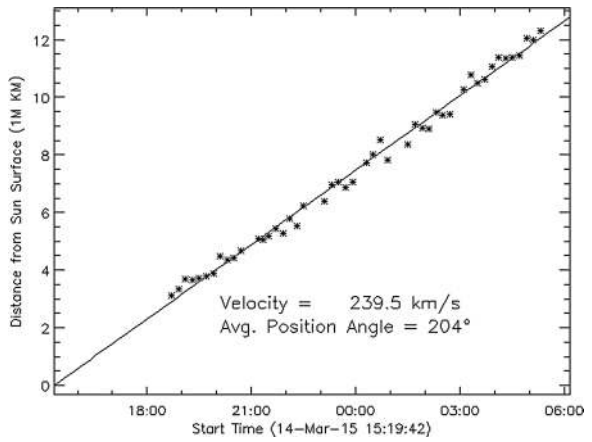

Fig. 8 Propagating speed of the CME14 in the FOV of C3 is ~240 km/s

from that of Liu et al. (2015) because: (1) there was no CME image available to confirm it, since CME14 and CME15 propagated out of the C3 FOV; (2) the CMEs' direction of propagation was different between CME14 (toward the south/bottom) and CME15 (toward the west/right); and (3) Fig. 7f–i shows clearly that CME14 was propagating in its own direction (southward projected on the plane of sky) after the leading edge of CME15 passed the leading edge of CME 14, showing no indication that CME14 and CME15 merged. Beside the above three points, the speed of CME14 was too slow (~240 km/s) to hit the Earth by 18 March 2015. It would take at least 7 days for CME14 to propagate from 7 Rs to the Earth, since the speed was 240 km/s. This means that CME14 would not hit the Earth by 21 March 2015. For these reasons, we concluded that the super-storm on 17 March 2015 was caused by the southward field in both the sheath and in part of MC17 which was driven by CME15.

One may argue that a slow CME will be accelerated by the ambient solar wind in interplanetary space. The propagating speed of CME14 was 240 km/s between 7–18 Rs. Assuming that CME14 was accelerated simultaneously to 300, 400, 500, 600, or 700 km/s at 06:06 UT on March 15 (see the last point in Fig. 8), it will take about 5.28, 3.96, 3.17, 2.64, or 2.26 days for the CME14 to arrive at the Earth, respectively. This means that CME14 could arrive at the Earth at around 12:48 UT on March 20; 05:12 UT on March 19; 10:12 UT on March 18; 21:29 UT on March 17; or 12:26 UT on March 17 for the CME14 with propagating speeds of 300, 400, 500, 600, 700 km/s, respectively. CME14 could be a candidate that caused the geomagnetic storm on 17 March 2015 if CME14 could be accelerated to 700 km/s near the Sun.

Conclusion

The first super geomagnetic storm of solar cycle 24 occurred on "St. Patrick's day" (17 March 2015). The source of the storm can be traced back to the solar event on 15 March 2015. At ~2:10 UT on that day, *SOHO/LASCO* C3 recorded a partial halo coronal mass ejection (CME), which was associated with a C9.1/1F flare (S22W25) and a series of type II/IV radio bursts. The propagation speed of this CME is estimated to be ~668 km/s for the period 02:10–06:20 UT (see Fig. 1). An interplanetary (IP) shock, likely driven by the related ICME, arrived at the *Wind* spacecraft at 03:59 UT on 17 March. We conclude that the St. Patrick's day event was a two-step storm. The first step was associated with the sheath, whereas the second step was associated with MC17. The solar source of MC17 was CME15.

We also found that choosing the correct Dst_{min} estimating formula for predicting the intensity of MC-associated geomagnetic storms is crucial for space weather predictions, because solar wind speed, as well as B_s, plays an important role in the prediction of geomagnetic activity.

Authors' contributions

CW designed and carried out the original study of the St. Patrick's Day event. She also wrote the first draft of the manuscript. KL performed data analysis and helped writing the manuscript. RL participated in the identification and data analysis of the MC and helped draft the manuscript. LH participated in the CME's measurement. SP participated in the interpretation of the evolution of the CME, and helped draft the manuscript. RH participated in the CME data analysis. DS participated in interpretation of CME's evolution and helped draft the manuscript. All authors read and approved the final manuscript.

Author details

[1] Naval Research Laboratory, Washington, DC 20375, USA. [2] Applied Physics Laboratory, Laurel, MD 20723, USA. [3] Emeritus, GSFC/NASA, Greenbelt, MD, USA.

Acknowledgements

We thank the *Wind* PI team and National Space Science Data Center at Goddard Space Flight Center for management and providing *Wind* plasma and magnetic field solar wind data. This study was supported partially by the Chief of Naval Research (CCW, SP, DS, LH). K.L. was supported by NASA grant NNX14AF83G to the Johns Hopkins University Applied Physics Laboratory. We acknowledge the support of NASA contract S-136361-Y for the STEREO/SECCHI effort. CCW has participated in the ISEST working group on the campaign events. CCW would like to thank VarSITI and ISEST for partial travel support.

Received: 12 March 2016 Accepted: 18 August 2016
Published online: 02 September 2016

References

Akasofu S-I (1981) Energy coupling between the solar wind and the magnetosphere. Space Sci Rev 28:121

Astafyeva E, Yasyukevich U, Maksikov A, Zhivetiev I (2014) Geomagnetic storms, super-storms, and their impacts on GPS-based navigation systems. Space Weather 12:508–525. doi:10.1002/2014SW001072

Echer E, Gonzalez WD (2004) Geoeffectiveness of interplanetary shocks magnetic clouds, sector boundary crossings and their combined occurrence. Geophys Res Lett. doi:10.1029/2003GL019199

Gonzalez WD, Joselyn JA, Kamide Y, Kroehl HW, Rostoker G, Tsurutani BT, Vasyliunas VM (1994) What is a geomagnetic storm? J Geophys Res 99(A4):5771–5792. doi:10.1029/93JA02867

Gopalswamy N, Akiyama S, Yashiro S, Xie H, Makela P, Michalek G (2015) The mild space weather in solar cycle. arXiv: 1508.01603.24

Hua L-N, Sonnerup BUO (1999) Two-dimensional coherent structures in the magnetospause: recovery of static equilibria from single-spacecraft data. J Geophys Res 104:6899–6918. doi:10.1029/1999JA900002

Kamide Y, Kusano K (2015) No major solar but the largest geomagnetic storm in the present solar cycle. Space Weather 13:365–367. doi:10.1002/2015SW001213

Kamide Y, Yokoyama N, Gonzalez W, Tsurutani BT, Daglis IA, Brekke A, Masuda S (1998) Two-step development of geomagnetic storms. J Geophys Res 103:6917–6922. doi:10.1029/97JA03337

Kataoka R, Shiota D, Keika E, Kilpua K (2015) Pileup accident hypothesis of magnetic storm on 17 March 2015. Geophys Res Lett 42:5155–5161. doi:10.1002/2015GL064816

Lakhina GS, Tsurutani BT (2016) Geomagnetic storms: historical perspective to modern view. Geosci Lett 3:5. doi:10.1186/s40562-016-0037-4

Lepping RP, Burlaga LF, Johnes JA (1990) Magnetic field structure of interplanetary magnetic clouds at 1 AU. J Geophys Res 95:11957. doi:10.1029/JA095iA08p11957

Lepping RP, Berdichevsky D, Ferguson T (2003) Estimated errors in magnetic cloud model fit-parameters with force free cylindrically symmetric assumptions. J Geophys Res 108:1356. doi:10.1029/2002JA009657

Lepping RP, Wu C-C, Berdichevsky DB (2005) Automatic identification of magnetic clouds and cloud-like regions at 1 AU: occurrence rate and other properties. Ann Geophys 23:2687–2704

Lepping RP, Berdichevsky DB, Wu C-C, Szabo A, Narock T, Mariani F, Lazarus AJ, Quivers AJ (2006) A summary of WIND magnetic clouds for years 1995–2003: model-fitted parameters, associated errors and classifications. Ann Geophys 24:215–245

Lepping RP, Wu CC, Berdichevsky DB, Szabo A (2015) *Wind* magnetic clouds for years 2010–2012: model parameter fittings, associated shock waves and comparisons to earlier periods. Sol Phys 290:2265–2290. doi:10.1007/s11207-015-0755-3

Liu Y, Luhmann JG, Bale SD, Lin RP (2011) Solar source and heliospheric consequences of the 2010 April 3 coronal mass ejection: a comprehensive view. Astrophys J. doi:10.1088/0004-637X/734/84

Liu YD, Hu H, Wang R, Yang Z, Zhu B, Liu YA, Luhmann JG, Richardson JD (2015) Plasma and magnetic field characteristics of solar coronal mass ejections in relation to geomagnetic storm intensity and variability. ApJL 809:1–6. doi:10.1088/2041-8205/809/2/L34

Marubashi K, Cho KS (2015) Non-uniqueness of the geometry of interplanetary magnetic flux ropes obtained from model-fitting. Sun Geospace 10:119–125

McAllister AH, Crooker NU (1997) Coronal mass ejections, corotating interaction regions, and geomagnetic storms. In: Crooker N, Joselyn JA, Feynman J (eds) Coronal mass ejections. Geophysics monograph series, vol 99. AGU, Washington, D.C, pp 279–289. doi:10.1029/GM099p0279

Möstl C, Farrugia CJ, Biernat HK, Leitner M, Kilpua EK, Galvin AB, Luhmann JG (2009) Optimized Grad–Shafranov reconstruction of a magnetic cloud using STEREO-Wind observations. Sol Phys 256:427–441. doi:10.1007/s11207-009-9360-7

Möstl C, Temmer M, Rollett T, Farrugia CJ, Liu Y, Vernoning AM, Leitner M, Galvin AB, Biernat HK (2010) STEREO and wind observations of a fast ICME flank triggering a prolonged geomagnetic storm on 5–7 April 2010. Geophys Res Lett. doi:10.1029/2010GL045175

Ramsingh, Sripathi S, Sreekumar S, Banola S, Emperumal K, Tiwari P, Kumar BS (2015) Low-latitude ionosphere response to super geomagnetic storm of 17/18 March 2015: results from a chain of ground-based observations over Indian sector. J Geophys Res 120:10864–10882. doi:10.1002/2015JA021509

Richardson IG, Cane H (2011) Geoeffectiveness (Dst and Kp) of interplanetary coronal mass ejections during 1995–2009 and implications for storm forecasting. Space Weather. doi:10.1029/2011SW000670

Tsurutani BT, Gonzalez WD (1997) The interplanetary causes of magnetic storms: a review. In: Tsurutani BT, Gonzalez WD, Kamide Y (eds) Geophysics monograph series, vol 98. American Geophysical Union, Washington, pp 77–89. doi:10.1029/GM098p0077

Tsurutani BT, Smith EJ, Gonzalez WD, Tang F, Akasofu SI (1988) Origin of interplanetary southward magnetic fields responsible for major magnetic storms near solar maximum (1978–1979). J Geophys Res 93:8517–8531. doi:10.1029/JA093iA08p08519

Wang YM, Zhou Z, Shen C, Liu R, Wang S (2015) Investigating plasma motion of magnetic clouds at 1 aU through a velocity-modified cylindrical force-free flux tope model. J Geophys Res 120:1543–1565

Wood BE, Wu C-C, Howard RA, Socker DG, Rouillard AP (2011) Empirical reconstruction and numerical modeling of the first geoeffective coronal mass ejection of solar cycle 24. Astrophys J 729:70. doi:10.1088/0004-637X/729/1/70

Wood BE, Lean L, McDonald SE, Wang Y-M (2016) Comparative ionospheric impacts and solar origins of nine strong geomagnetic storms in 2010-2015. J Res Geophys. doi:10.1002/2015JA021953

Wu C-C, Lepping RP (2002a) Effects of magnetic clouds on the occurrence of geomagnetic storms: the first 4 years of *Wind*. J Geophys Res. doi:10.1029/2001JA000161

Wu C-C, Lepping RP (2002b) Effect of solar wind velocity on magnetic cloud-associated magnetic storm intensity. J Geophys Res 107(A11):1346. doi:10.1029/2002JA009396

Wu C-C, Lepping RP (2005) Predicting magnetic cloud related geomagnetic storm intensity. J Atmos Terr Phys 67:283–291. doi:10.1016/j.jastp.2004.07.040

Wu C-C, Lepping RP (2008) Geomagnetic activity associated with magnetic clouds, magnetic cloud-like structures and interplanetary shocks for the period 1995-2003. Adv Space Rev 41:335–338. doi:10.1016/j.asr.2007.02.027

Wu CC, Lepping RP (2011) Statistical comparison of magnetic clouds with interplanetary coronal mass ejections for solar cycle 23. Solar Phys 269:141–153. doi:10.1007/s11207-010-9684-3

Wu CC, Lepping RP (2015) Statistical comparison of magnetic clouds and cloud-like structures during 1995–2012. Solar Phys 290:1243–1269. doi:10.1007/s11207-015-0656-5

Wu C-C, Lepping RP (2016) Relationships among geomagnetic storms, interplanetary shocks, magnetic clouds, and sunspot number during 1995–2012. Sol Phys 291:265–284. doi:10.1007/s11207-015-0806-9

Wu C-C, Gopalswamy N, Lepping RP, Yashiro S (2013) Characteristics of magnetic clouds/interplanetary coronal mass ejections which caused intense geomagnetic storms. Terr Atmos Ocean Sci 24(2):233–241. doi:10.3319/TAO.2012.09.26.03

Wu C-C, Liou K, Vourlidas A, Plunkett S, Dryer M, Wu ST, Socker D, Wood BE, Hutting L, Howard R (2016a) Numerical simulation of multiple CME-driven shocks in the month of 2011 September. J Geophys Res 121:1839–1856. doi:10.1002/2015JA021843

Wu C-C, Liou K, Vourlidas A, Plunkett S, Dryer M, Wu ST, Mewald RA (2016b) Global Magnetohydrodynamic simulation of the March 15, 2013 coronal mass ejection event—interpretation of the 30–80 MeV proton flux. J Geophys Res 121:56–76. doi:10.1002/2015JA021051

Zhang J, Richardson IG, Webb DF, Gopalswamy N, Huttunen E, Kasper J, Nitta N, Poomvises W, Thompson BJ, Wu C-C, Yashiro S, Zhukov Z (2007) Solar and interplanetary sources of major geomagnetic storms (Dst < = - 100 nT) during 1996 - 2005. J Geophys Res 112:A10102. doi:10.1029/2007JA012321